Carbazole-substituted benzobisoxazoles: near-UV fluorescent emitters and ambipolar hosts for organic light-emitting diodes†

David L. Wheeler,[a] Lloyd Fisher Jr,[f] Pascal Friederich, [ID][cde] Christopher Cunningham,[a] Angelar K. Muthike,[f] Alán Aspuru-Guzik,[cd] Theodore Goodson III [ID][f] and Malika Jeffries-EL [ID] *[ab]

The design of organic light emitting diode (OLED) materials with the potential for exhibiting thermally-activated delayed fluorescence (TADF) is reported. Using computational methods (DFT/TD-DFT) as a guiding tool, six materials with a benzobisoxazole (BBO) core and donor–acceptor–donor architectures were designed by changing the conjugation position of carbazole-substituted phenyl substituents and the type of BBO isomer (cis- vs. trans-). Experimental steady-state and transient absorption spectroscopic techniques were utilized to probe the TADF activity of these molecules. Each material was then used in host–guest OLED devices as either near-UV dopants or host with low singlet-triplet energy differences. The electroluminescent properties show that when used as dopants these materials provide near-UV emission (CIE_y < 0.06 and CIE_x = 0.16), whereas when used as hosts, these materials show reduced operating voltages and increased performance efficiencies when compared to commercial materials.

Introduction

In recent years, there has been a renewed interest in organic light emitting diodes (OLEDs) due to their potential for the development of next-generation devices such as flexible displays,[1] wearables[2] and solid-state lighting.[3] OLEDs have several advantages over conventional inorganic LEDs including the ability to fabricate them onto either rigid or flexible substrates, to accommodate irregular surfaces. They can also be fabricated almost entirely from solution-processing techniques, eliminating the need for energy-intensive fabrication methods such as thermal evaporation. OLEDs can also be used to make lightweight displays since they do not require backlighting.

Purely organic luminophores are promising because, these molecular or polymeric organic semiconductors (OSC)s can be modified through organic synthesis to produce materials with optical and electronic properties tailored for targeted applications.[4] OSCs also eliminate the need for toxic, expensive noble metals. However, achieving deep blue emission within the industry standards for color purity: National Television System Committee (NTSC) (CIE: 0.14, 0.08) and European Broadcasting Union (EBU) (CIE: 0.15, 0.06) using a purely organic emitter is challenging.[5] Further, since fluorescence OLEDs utilize singlet emission, the theoretical maximum internal quantum efficiencies (IQE) based on these materials is limited to 25% since the ratio of singlets and triplet generated under electroluminescent conditions is 1:3.[6] One solution to overcoming the theoretical limit for fluorescence is through the design of emitters that exhibit thermally activated delayed fluorescence (TADF).[7] Such materials can theoretically achieve an IQE of 100% through a process known as reverse intersystem crossing (rISC). This process converts non-emissive excited triplet (T_1) excitons into emissive excited singlet state (S_1), albeit at a lower rate than intersystem crossing ($S_1 \rightarrow T_1$). By engineering materials with good charge-transfer (CT) character, one can reduce the energetic difference between the S_1 and T_1 states (ΔE_{ST}), increasing the rate of rISC (k_{rISC}) thereby inducing TADF.[8] This is typically accomplished by spatially separating the highest occupied molecular orbital (HOMO) and lowest unoccupied molecular orbital (LUMO) within a flurophore.[9]

Our group has been developing tunable OSCs based on the benzo[1,2-d:4,5-d']bisoxazole (BBO) ring system, Fig. 1. This electron-deficient heterocycle can readily be substituted with

[a] Department of Chemistry, Boston University, 590 Commonwealth Ave, Boston, MA 02215, USA. E-mail: malikaj@bu.edu

[b] Division of Materials Science and Engineering, Boston University, 15 St Mary's St. #117, Boston, MA 02215, USA

[c] Department of Chemistry, University of Toronto, 80 St George St, Toronto, ON M5S 3H6, Canada

[d] Department of Computer Science, University of Toronto, 214 College St, Toronto, ON M5T 3A1, Canada

[e] Institute of Nanotechnology, Karlsruhe Institute of Technology, Hermann-von-Helmholtz-Platz 1, 76344 Eggenstein-Leopoldshafen, Germany

[f] Department of Chemistry, University of Michigan, Ann-Arbor Michigan 48109-1055, USA
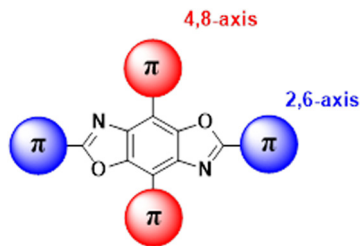
Fig. 1 General structure of the BBO core. Conjugation can take part at the 2 and 6 positions (axis) or the 4,8 axis.

various aryl substituents in two ways: through the oxazole rings (2,6-axis) and/or the central benzene ring (4,8-axis). As a result, the BBO moiety can be used as a platform to design a multitude of materials with varying opto-electronic properties, using simple, scalable synthons.[10–13] Moreover, many aryl-substituted BBOs are highly fluorescent materials that are stable under ambient atmosphere and at high temperatures, making them ideal candidates for use in OLEDs.[14,15] Lastly, many aryl-BBOs possess spatially segregated frontier molecular orbitals (FMO)s, which is favorable for achieving a small ΔE_{ST}.[13,16] Previously, we reported a series of small-molecule BBO dopants which were used in host–guest OLEDs that exhibited deep-blue electroluminescence (EL) ($^{EL}\lambda_{max} \approx 440$ nm; $CIE_y < 0.10$), albeit with external quantum efficiencies (EQE)s less than 3%.[14] The low efficiency of the devices was attributed in part to the traditional fluorophore character of the BBO dopants where ∼75% of the excitons created were lost to various non-radiative pathways. Recently, we examined how steric hindrance impacts the opto-electronic properties of a series of aryl-substituted BBOs.[12] While theoretical predictions demonstrated that a considerable amount of overlap was observed between the HOMO and LUMO, the materials did show potential for usage as for blue host and emissive materials.

In this work, we endeavored to develop TADF emitters by functionalizing the BBO core with electron-rich carbazole pendants. Carbazole was selected as a substituent because of its high triplet energy and good hole-transporting abilities.[17] Accordingly, using computational and experimental methods, a series of six BBOs were designed with a donor–acceptor–donor (DAD) architecture to help reduce the ΔE_{ST}. Of the six systems, compounds **C1**, **C3**, and **C5** bore BBO cores with 4-(*N*-carbazol-9-yl)phenyl- substituents while **C2**, **C4**, and **C6** contained 3,5-di(*N*-carbazol-9-yl)phenyl groups. Unfortunately, despite the predictions, experimental results indicate that none of the materials were TADF-active. However, each material was able to be employed into host–guest OLED devices functioning as either fluorescent dopants or ambipolar hosts and are promising precursors for designing BBO-based TADF emitters.

Results and discussion

Computational predictions

The study began by modelling the six materials of interest using DFT/TD-DFT to determine the optimized geometries and predict optical and electronic properties (Table 1). Due to their similarities in structure, compounds **C1**, **C3**, and **C5** are referred to as

Table 1 Computed electronic and geometric properties of the six BBO materials

| BBO | Electronic properties | | | | | Dihedral angles | |
	HOMO (eV)	LUMO (eV)	E_g^{opt} (eV)	ΔE_{ST} (eV)	f	2,6 (°)	4,8 (°)
C1	5.20	1.74	3.06	0.64	8.8×10^{-1}	—	29.6
C2	5.39	1.96	3.01	0.46	1.8×10^{-2}	—	33.7
C3	5.39	2.01	2.96	0.59	1.5×10^{00}	0.5	—
C4	5.50	2.26	2.83	0.38	4.1×10^{-2}	4.5	—
C5	5.42	1.93	3.06	0.47	1.3×10^{00}	3.9	—
C6	5.50	2.15	2.92	0.22	1.3×10^{-2}	1.0	—

the di-substituted carbazole (DC) group while the tetra-substituted carbazole (TC) group includes compounds **C2**, **C4** and **C6**. By altering the connection and orientation of the carbazole rings relative to the BBO core, we hoped to identify trends leading to materials with small ΔE_{ST}.

We began the analysis by recognizing structure-property relationships between the HOMO levels of each material. All BBO systems in the DC group were found to have HOMO energies between -5.2–-5.4 eV while those in the TC group are slightly lower between -5.4–-5.5 eV. The similarity in HOMO energies within each group is due to the comparative localization of electron density between the three BBOs (Fig. 2). However, the electron density for the DC group compounds is more delocalized compared the TC group. Furthermore, the
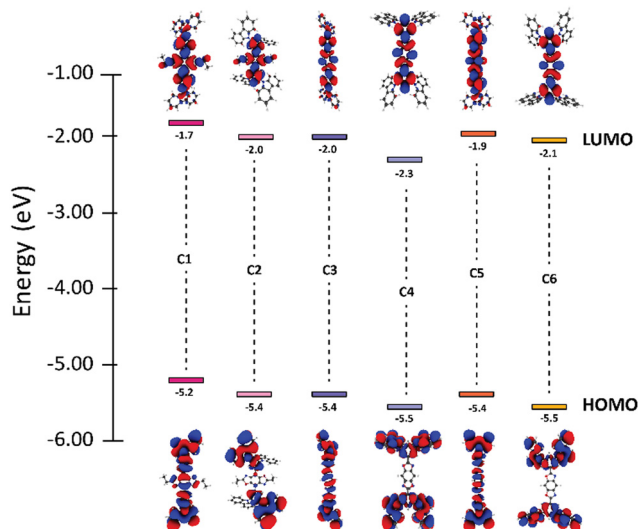

Fig. 2 FMOs and electronic energy levels of **C1–C6**.

HOMO energies of the DC-BBOs **C1**, **C3**, and **C5** are also computed to be slightly higher than the HOMO of their respective TC group partners. This delocalization and energetic increase can be attributed to the substituent position within the pendant carbazole relative to the BBO core. For the DC group materials, the lone-pair electrons on the carbazole nitrogen are in direct conjugation to the BBO core when conjugated at the *para*-position while the *meta*-conjugation of the TC systems force these groups to be electronically orthogonal. Independent of the carbazole substitution, when the aryl substituents are substituted through the 4,8-axis of the BBO core, a slight increase in the HOMO energy is observed compared to those conjugated through the 2,6-axis. According to the computations, there is negligible change in the HOMO energy whether the BBO core is the *trans*- or *cis*- isomer.

Next, trends between the LUMOs of each compound were analysed. The LUMO energy for the DC group is found to range between −1.7−−2.0. The LUMO energy is lowered slightly for the TC group, ranging between −2.0−−2.3 eV. The degree of separation between the HOMO and LUMO is more pronounced in the TC group than the DC group due to the conjugation position of the carbazole units. The axis of conjugation also affects the LUMO energy as **C1** is found to be 0.2–0.3 eV higher in energy compared to **C3** and **C5**. A similar result is found comparing **C2** to both **C4** and **C6**. Unlike the HOMO, inclusion of the *cis*-core restricts the conjugation pathway of pi-electrons, thereby increasing the LUMO energy by 0.1–0.2 eV.

The band gaps for all BBOs were found to be suitable for use as deep blue emissive materials or wide bandgap hosts due to their short conjugation pathways (3.1–2.8 eV). Interestingly, the computations show compounds in the TC group have smaller band gaps when compared to their respective DC partners. This can be attributed to the higher CT character of compounds **C2**, **C4**, and **C6** which has significant impact on lowering the LUMO. As a result, these materials not only have a smaller band gap, but also a smaller ΔE_{ST} when compared to their DC partners. However, the S_1 oscillator strengths for compounds **C2**, **C4**, and **C6** are low $(<10^{-1})$ compared to **C1**, **C3** and **C5**, indicating the TC materials may not be as luminescent as their DC counterparts. Nonetheless, apart from **C1** and **C3**, all compounds were calculated to exhibit $\Delta E_{ST} < 0.50$ eV, which is favorable for TADF. With this knowledge, each compound was then synthesized to determine the experimental optical and electronic properties.

Synthesis and characterization

The BBOs were synthesized using a simple three-step process, minimizing the need for inert atmosphere. The precursors were formed using the pathway outlined in Scheme 1. All precursor materials were formed starting from commercially available fluorinated benzonitrile or bromobenzene derivatives. First, the commercial materials were heated with stoichiometric amounts of carbazole and potassium *tert*-butoxide in *N,N*-dimethylformamide under normal atmosphere to produce the carbazole-substituted bromobenzene (**1**; 86% and **2**; 65%) and benzonitrile (**3**; 78% and **4**; 71%) derivatives in moderate yields. Compounds **1**
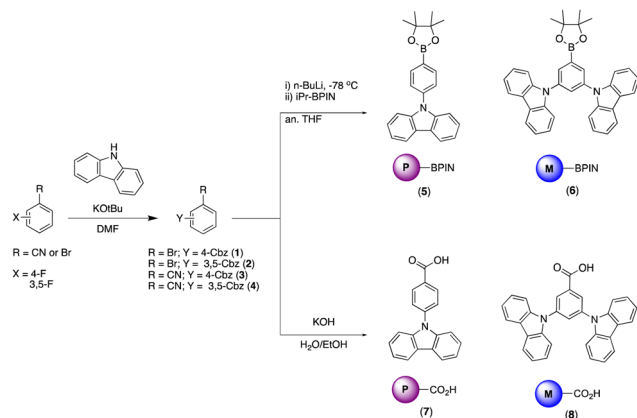
Scheme 1 Synthesis of precursor material **1–8**.

and *tert* were dissolved in anhydrous tetrahydrofuran (THF), lithiated with *n*-butyllithium, and quenched with 2-isopropoxy-4,4,5,5-tetramethyl-1,3,2-dioxaborolane to produce the desired boronic esters **5** (79%) and **6** (60%). Compounds **3** and **4** were hydrolysed under normal atmosphere using an aqueous 6 M sodium hydroxide solution and reagent alcohol to produce nearly quantitative yields of the substituted benzoic acid derivatives **7** (95%) and **8** (89%).

The final step synthesis is illustrated in Scheme 2. We elected to use high-pressure Suzuki-Miyaura conditions to form the 4,8-conjugated BBOs due to its low toxicity and effectiveness based off previous work.[12] Using cesium fluoride as the base and THF as the solvent, **C1** and **C2** were produced in yields of 60% and 37%, respectively. Lastly, the 2,6-conjugated BBOs were formed through a condensation technique using polyphosphoric acid trimethylsilyl ester (PPSE) as a desiccant with either 2,5-diaminohyroquinone bis-hydrochloride or 4,6-dinitroresorcinol, producing **C3–C6** (28–38% yields). All compounds exhibit decent-to-low solubility in chlorinated solvents and where structurally characterized using NMR and high-resolution MS (ESI) techniques.

Electronic properties

The theoretical and experimental electronic properties of **C1–C6** are listed in Table 2. The experimental HOMO energies were calculated using ionization potentials determined from ultraviolet photoelectron spectroscopy (UPS). We chose this technique over cyclic voltammetry due to its ability to measure the work function of materials with high accuracy. Further, many of the BBOs were not soluble in suitable solvents for electrochemistry. The optical HOMO → LUMO transition energies (E_g^{opt}) were determined from the onset of each thin-film UV-Vis spectrum. LUMO levels were then calculated by adding the E_g^{opt} to the experimental HOMO energies.

In all cases, the HOMO and LUMO levels measured are similar to common commercial hosts/emitters for blue OLEDs. All experimental HOMO energies range from −6.1 to −5.8 eV, which are 0.3–0.7 eV deeper than the computationally predicted values. Similarly, the theoretical LUMO values (−2.3 to −1.7 eV)
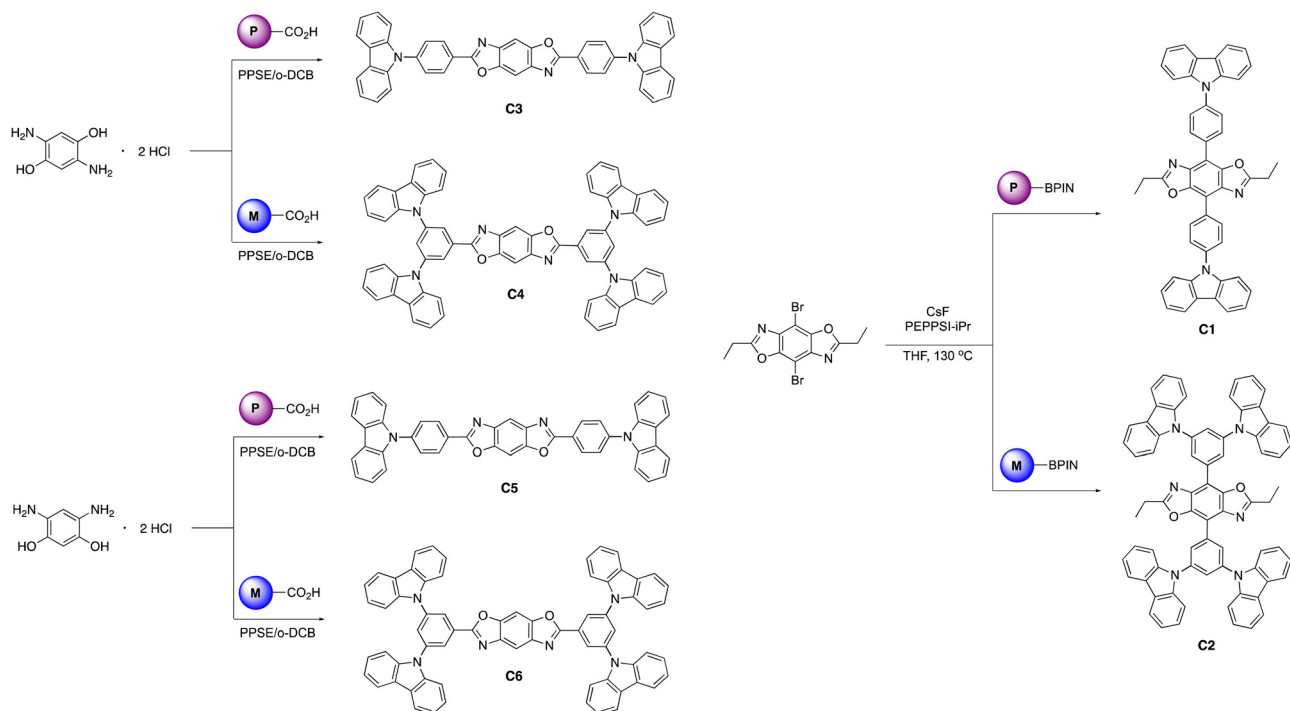
Scheme 2 Synthesis of final molecules **C1–C6**.

Table 2 Measured steady-state optical and electronic properties for BBOs **C1–C6**

| | Optical properties | | | | | | | Electronic properties | | |
| | Solution | | | | | Thin film | | | | |
BBO	ε (10^4) (M^{-1} cm^{-1})	$^{abs}\lambda_{max}$ (nm)	$^{em}\lambda_{max}$ (nm)	Φ (%)	ΔE_{ST} (eV)	$^{abs}\lambda_{max}$ (nm)	$^{em}\lambda_{max}$ (nm)	HOMO^a (eV)	LUMO^b (eV)	E_g^c (eV)
C1	3.4	**347**	**415**	68	0.59	**363**	**424**, 445	5.9	2.9	3.0
C2	5.7	313, **326**, 340	**428**	10	0.22	**329**, 342	**419**	6.1	2.8	3.3
C3	6.0	**372**, 388	**416**, 433	42	0.46	**380**, 401	423, **448**, 470	6.0	3.1	2.9
C4	6.9	337, 351, **370**	**448**	3.9	0.47	329, **340**	**437**	5.8	2.7	3.1
C5	5.4	**363**, 377	**414**	27	0.64	**369**, 388	**436**	6.0	3.0	3.0
C6	7.6	327, **341**, 360	**440**	4.8	0.38	329, **340**	**435**	5.9	2.7	3.2

Bold values indicate wavelength of maximum absorbance/emission. ^{a} Measured using UPS. ^{b} Estimated using the following equation: LUMO = HOMO + E_g. ^{c} Calculated from onset of absorbance.

are calculated to be 0.5–1.2 eV higher in energy than the experimental values (−3.1 to −2.7 eV). The experimental E_g^{opt} suggest excellent potential as host/emitter materials for blue OLEDs as all compounds ranged from 2.9 to 3.3 eV. These values are in good agreement with computational findings (abs. diff. ≤0.3 eV). For BBOs **C1**, **C3**, and **C5**, the E_g^{opt} are lower in energy when compared to their 3,5-disubstituted analogues. This observation is attributed to the *para*-conjugation of each carbazole to the benzene ring, allowing the non-bonding electron pair of the heteroatom to contribute to the extended pi-system.

Steady-state optical properties

The optical property investigation began by analysing the steady-state absorbance and emission profiles of **C1–C6**. Each compound was examined as a 0.01 g L^{-1} solution dissolved in chloroform (Fig. 3) and as a thin film (see ESI†). We first examined the difference in absorption profiles between BBOs in solution. In all cases, two main absorption bands characteristic of chromophores with donor–acceptor configurations, demonstrating their CT nature.[18,19] The high energy bands can be ascribed to the localized excitations due to π–$\pi^\star$ transition of the moieties, while the low energy bands can be ascribed to the n–$\pi^\star$ charge transfer transition among the moieties.[18,20] It is interesting to note that the more prominent CT absorption band is obtained from the systems with DC compounds rather than the TC systems. One would expect that **C2**, **C4**, and **C6** would exhibit higher donor strength and yield more prominent charge transfer features.[21] However, the multiple carbazole subunits of the **C2**, **C4**, and **C6** materials make the localized absorption transition more prominent. Of all materials, the DC group BBOs show bathochromic absorption when compared to the TC systems. This is a direct consequence of the lower E_g^{opt} and substitution pattern of carbazole units for **C1**, **C3**, and **C5**.
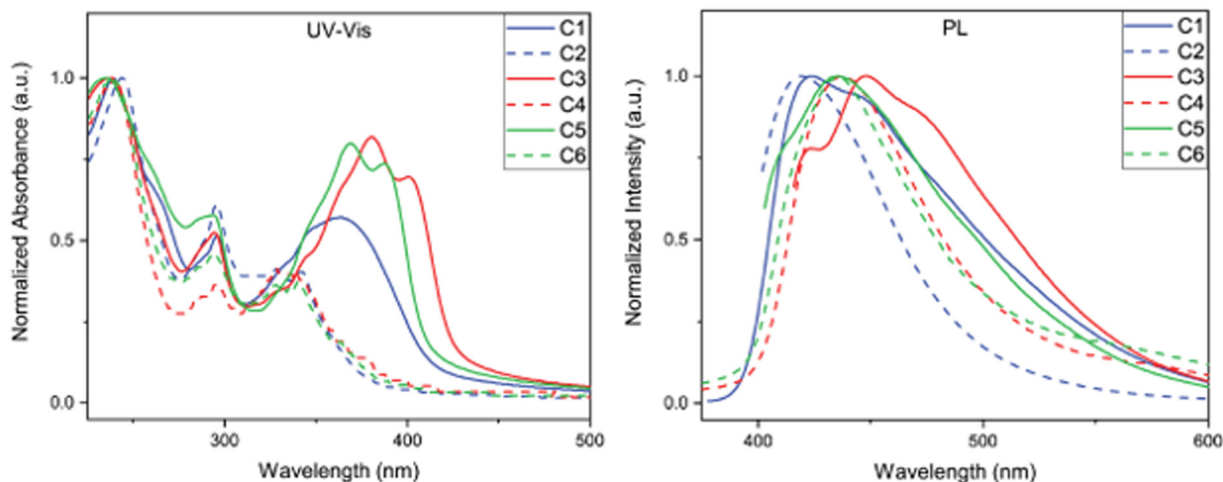
Fig. 3 Steady-state absorbance spectra of **C1–C6** in chloroform (left) at 0.01 g L^{-1} and photoluminescence spectra of **C1–C6** thin-film (right).

Compounds which contain the *cis*-isomeric core exhibit hypsochromic shift in absorption relative to the BBOs with the *trans*-moiety. When the aryl substituents are conjugated through the 4,8-axis, an enhanced hypsochromic shift is observed compared to the BBOs with 2,6-axis substituents. This is attributed to the increased dihedral angle that exists between the BBO core and aryl substituent, as supported from DFT calculations (Table 1). As thin films, **C1**, **C3**, and **C5** still demonstrate a bathochromic shift in absorption when compared to their TC group partners. While changing the *cis*-core to the *trans*-isomer provides a red-shift in absorbance, this effect is not as intense when compared to the same observation in solution.

The photoluminescence (PL) spectra were measured to determine emission profiles and quantum yields for each BBO (Fig. 2 and Table 2). In solution, **C1**, **C3**, and **C5** all produce emission at approximately 415 nm with quantum yields ranging from 27–68%. A secondary peak at 433 nm is observed for **C3** but is not observed for the structural isomer, **C5**. For the TC systems, the experimental observations closely matched the DFT predictions as the emission intensities of these materials are low with broad profiles and quantum yields ranging from 3–10%. When measured as thin films, all compounds were found to exhibit emission maxima between 419–448 nm. The emission profiles for **C1**, **C3**, and **C5** broaden and produce bathochromic emission compared to their solution-state spectra. These observations are attributed to each compound's ability to undergo π–π stacking readily. Conversely, **C2**, **C4**, and **C6** undergo slight hypsochromic emission with little change in peak breadth. Due to the bulky nature of these compounds, we believe the pi-systems of each molecule are unable to interact effectively in a macroscopic environment, thereby producing similar emission profiles when compared to their solution spectra. This property is expected to be highly beneficial for bipolar host material that can facilitate energy-transfer without radiative quenching.

The quantum yields (ϕ) of the investigated compounds were analysed in both unpurged and purged chloroform solutions (see ESI†). In the case of the **C5**, a ϕ value (27%) was obtained in unpurged solution. An appreciable ϕ enhancement was also obtained for the **C5** chromophore after purging oxygen from the solution (33%). It has been suggested that the difference of the ϕ before and after the oxygen purging process is due to excited state dynamics governed by a delayed fluorescence mechanism.[22] Contrarily to **C5**, a very small ϕ (4.8%) was obtained for **C6**, which suggests a poor fluorescence decay in oxygen-rich environments but is enhanced when oxygen is expelled from the solution (6.2%).[18] Such a small enhancement indicates that other decay pathways for the excited states outcompete fluorescence decay. Similar results were obtained for the remaining mono-carbazole donor moiety emitters and their respective bi-carbazole donor moiety counterparts. Based on these results, we sought to further investigated these compounds using time-resolved techniques at the nanosecond timescale.

Nanosecond transient absorbance

Transient absorption (TA) spectra of the investigated compounds were obtained to gain insight into their emissive mechanism (Fig. 4). In each spectrum, positive ΔOD peaks are representative of excited state absorption (ESA) while negative peaks are representative of either ground state bleaching (GSB) or stimulated emission (SE). The lifetimes of each peak were then investigated to aid in determining what emissive mechanisms are accessible by these compounds. Each TA spectrum of the mono-carbazole donor DC emitters display a SE peak that is in good agreement with the steady-state fluorescence results (Table 3). No other peaks are readily observable, indicating that the lifetime of both the GSB and ESA are below the time resolution of this technique. This suggests that fluorescence emission is efficient for these compounds and outcompetes other radiative decay pathways.

Contrary to **C1**, **C3**, and **C5**, the TA spectra of the bi-carbazole donor TC emitters display a GSB, SE, ESA, and a third negative peak. To determine the lifetime of the ESA and third negative peak, transient decay traces were obtained (see ESI†). For **C6**, the ESA lifetime (430 nm) in unpurged chloroform is 632 ns, which is a longer timescale compared to typical singlet states. However, this lifetime is enhanced with oxygen purging, increasing the
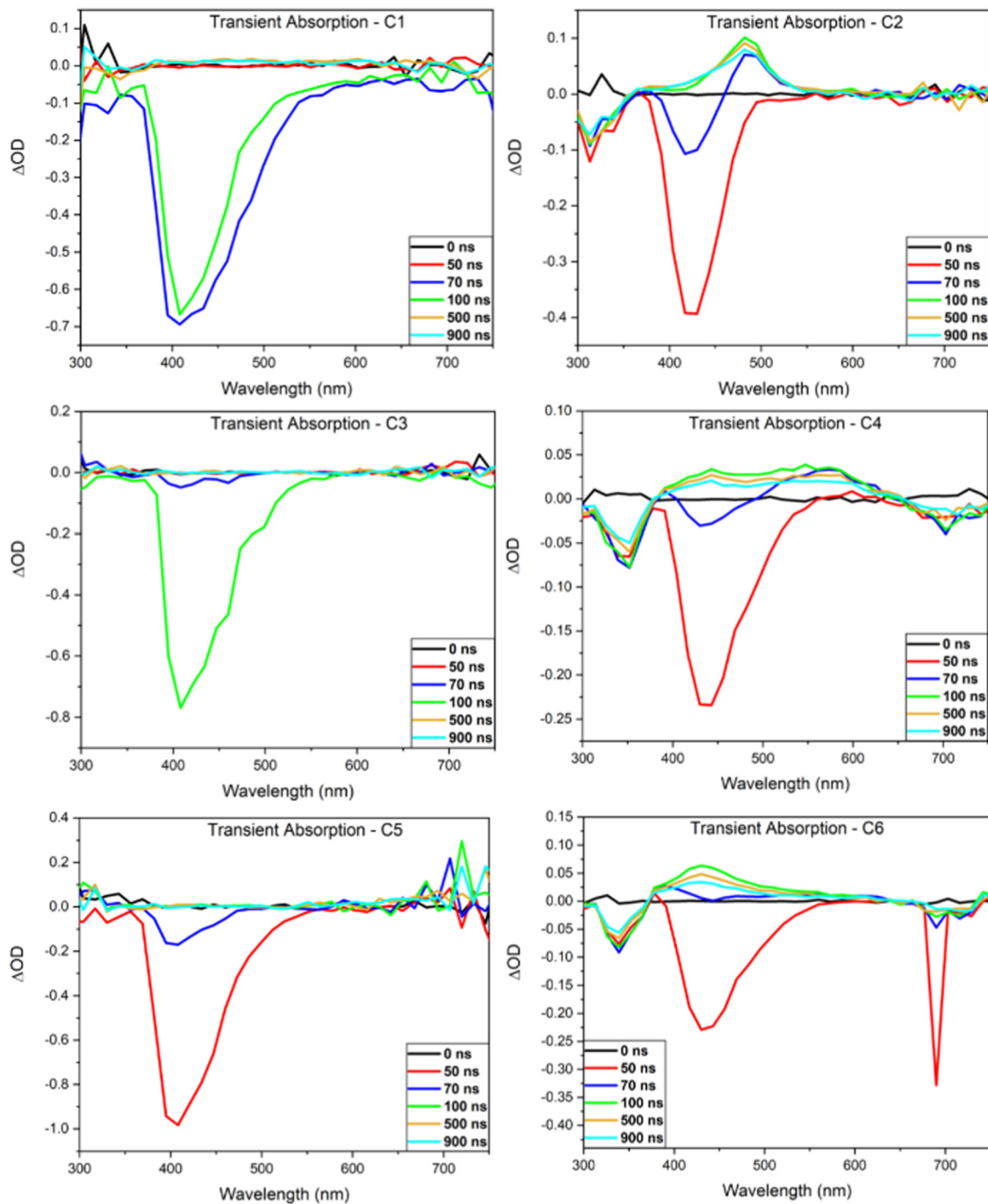
Fig. 4 Nanosecond transient absorption spectra of the six BBOs.

timescale just nearly into the microsecond regime (992 ns), indicating that this state has significant triplet character. Similar results are obtained for the third negative peak at ∼700 nm observed after 70 ns (Fig. 4) which has a lifetime of 576 ns in the oxygenated solution. However, this peak is not indicative of GSB or SE as GSB is observed at ∼340 nm and overlaps well with the steady-state absorption spectrum while SE is observed at ∼430 nm and overlaps well with the steady-state emission spectrum. Thus, we determine that this state is representative of phosphorescence emission. The significant enhancement of

this state's lifetime with oxygen purging to 1152 ns supports this, as oxygen is known to quench the triplet state. These lifetimes match well with that of the ESA in both the oxygenated and oxygen-purged solutions, suggesting that this emission is the result of the ESA decay. It should be noted that the sharp peak observed at ∼700 nm at 50 ns is the result of the second harmonic of the excitation beam and not emission of **C6**. Similar results were obtained for **C2** and **C4** with the most noticeable difference being that both emitters have longer ESA and phosphorescence lifetimes than **C6** (Fig. S20, ESI†).

Table 3 Transient properties and kinetic traces of the TC group BBOs

BBO	GSB (nm)	SE (nm)	ESA (nm)	k_{rISC} (s^{-1})	τ_{ESA} (s)	k_{ESA} (s^{-1})	τ_{Ph} (s)	k_{Ph} (s^{-1})
C1	—	410	—	—	—	—	—	—
C2	325	424	487	4.30×10^4	1.16×10^{-6}	8.59×10^5	1.92×10^{-6}	5.21×10^5
C3	—	408	—	—	—	—	—	—
C4	350	438	547	5.68×10^3	1.41×10^{-6}	7.10×10^5	1.54×10^{-6}	6.51×10^5
C5	—	408	—	—	—	—	—	—
C6	340	430	430	1.41×10^4	9.92×10^{-7}	1.01×10^6	1.15×10^{-6}	8.68×10^5

GSB = ground state bleaching. SE = stimulated emission. ESA = excited state absorbance. k_{rISC} = reverse intersystem crossing rate. KESA = ESA rate. KPh = rate of phosphorescence. τ_{ESA} = ESA lifetime. τ_{Ph} = phosphorescence lifetime.

The ESA lifetime results were used to calculate the rate of reverse intersystem crossing (k_{rISC}) and determine if any of the emitters are capable of TADF.[19,23] No k_{rISC} could be determined for the DC emitters, as they possessed no ESA that could be measured by the nanosecond TA technique. Based on the timescale of relaxation, we believe **C1**, **C3**, and **C5** to be traditional fluorophores. The k_{rISC} values calculated for the TC emitters are displayed in Table 3 along with the rate of phosphorescence (k_{phos}). Both k_{rISC} and k_{phos} compete for the triplet ESA, where k_{phos} values are an order of magnitude greater than the k_{rISC} results, in all cases. Therefore, it is determined that the TC emitters are more efficient phosphorescent compounds than TADF compounds.

Based on the steady-state and transient spectral data, it is evident that **C1**, **C3**, and **C5** exhibit properties useful as fluorescent dopant materials as seen in their PL spectra and moderate-to-high PLQYs in oxygen-free environments. Unfortunately, none of the BBO materials display any TADF characteristics. Conversely, **C2**, **C4**, and **C6** show quite narrow ΔE_{ST} and long-lived triplet lifetimes before phosphorescence decay (+1 μs). While the rate of k_{rISC} is an order of magnitude smaller than the k_{phos}, these materials do not exhibit bright emission and could be useful as potential BBO-based phosphorescent/TADF host materials. Therefore, **C1**, **C3**, and **C5** were optimized into solution processed devices as active layer materials while **C2**, **C4**, and **C6** were paired with commercial TADF emitter 2,3,4,5,6-pentakis(3,6-di-*tert*-butyl-9H-carbazol-9-yl)benzonitrile (5TCzBN) to evaluate preliminary results as ambipolar hosts.

Device properties

We studied OLED characteristics of **C1**, **C3**, and **C5** as solution-processed dopants in a mixed host matrix. The device architecture consisted of the following: ITO (100 nm)/PEDOT:PSS (35 nm)/Active Layer (mixed host: 5% BBO)/TmPyB (35 nm)/LiF (1 nm)/Al (100 nm). Shown in Fig. 5 is the band diagram of all active layer materials and efficiency graphs while Table 4 collates the EL properties of the devices using BBO-based dopants.

The EL spectra of each dopant exhibit a relatively minor red-shift when compared to their solution-state PL spectrum. Of the three dopants, **C5** was found to exhibit the most blue-shifted emission of the set at 405 nm, with a second band at 424 nm. **C1** and **C3** show emission maxima at 413 nm and 417 nm, respectively. The peak widths at half max for all EL spectra were less than 55 nm, indicating good color purity for organic molecules. Furthermore, all three dopants exhibit CIE_y values <0.06 and CIE_x values of 0.16. While these compounds nearly meet the National Television Systems Committee and European Broadcasting Union's requirements for deep-blue emission, the larger CIE_x value indicates near-UV emission, providing a purple hue to the emitted light. Each device demonstrates operating voltages (measured at 100 cd m^{-2}) less than 4.8 V and max luminance between 300–900 cd m^{-2}. The best performing dopant of the set was **C3**, achieving a current efficiency (CE) of 0.53, power efficiency (PE) of 0.34, and a max EQE of 0.88. While small, the efficiencies of all materials are comparable to other materials which emit near UV emission using identical doping concentrations.[24] While specific measurements would be required for support, we attribute the low EQE of these devices to the emission mechanism of the molecule and the traditional host guest architecture of the system. However, two methods of overcoming the latter argument would be to employ these systems into (1) a thermally evaporated device with (2) the use of a TADF-sensitizer to obtain near-UV hyperfluorescence emission. Unfortunately, due to the constraints of the thermal evaporator, this architecture could not be obtained. These architectures will be investigated in the future, when possible.

We next preliminarily evaluated **C2**, **C4**, and **C6** as a host material. Each system was thermally evaporated with the commercial TADF dopant, 5TCzBN. The device architecture used was ITO (100 nm)/PEDOT:PSS (35 nm)/Active Layer (host: 20% 5TCzBN)/TmPyPB (35 nm)/LiF (1 nm)/Al (100 nm). BBOs **C2**, **C4**, and **C6** produced more promising results when compared to the device using the commercial *m*CP host. Demonstrated by the RMS values from AFM measurements (see ESI†), the TC group show very similar active layer morphologies, resulting in hosts which do not alter the emission maxima by more than 5 nm. However, the BBO hosts drastically reduce the operating voltage by as much as 4.0 V when compared to the device using *m*CP as the host. We hypothesize that this is due to the ambipolar nature of the materials, which can provide better energetic agreement between the LUMO levels of the host and dopant. As a result, the BBO hosts were able to attain higher CE, PE and EQEs while some produced comparable brightness when compared to the *m*CP device. From these preliminary devices, the BBO materials indicate great potential as hosts due to their improved operating voltages and efficiencies when compared to commercially available *m*CP.

Conclusions

In summary, six BBO materials with a DAD motif were computationally modelled to evaluate their potential as TADF emitters.
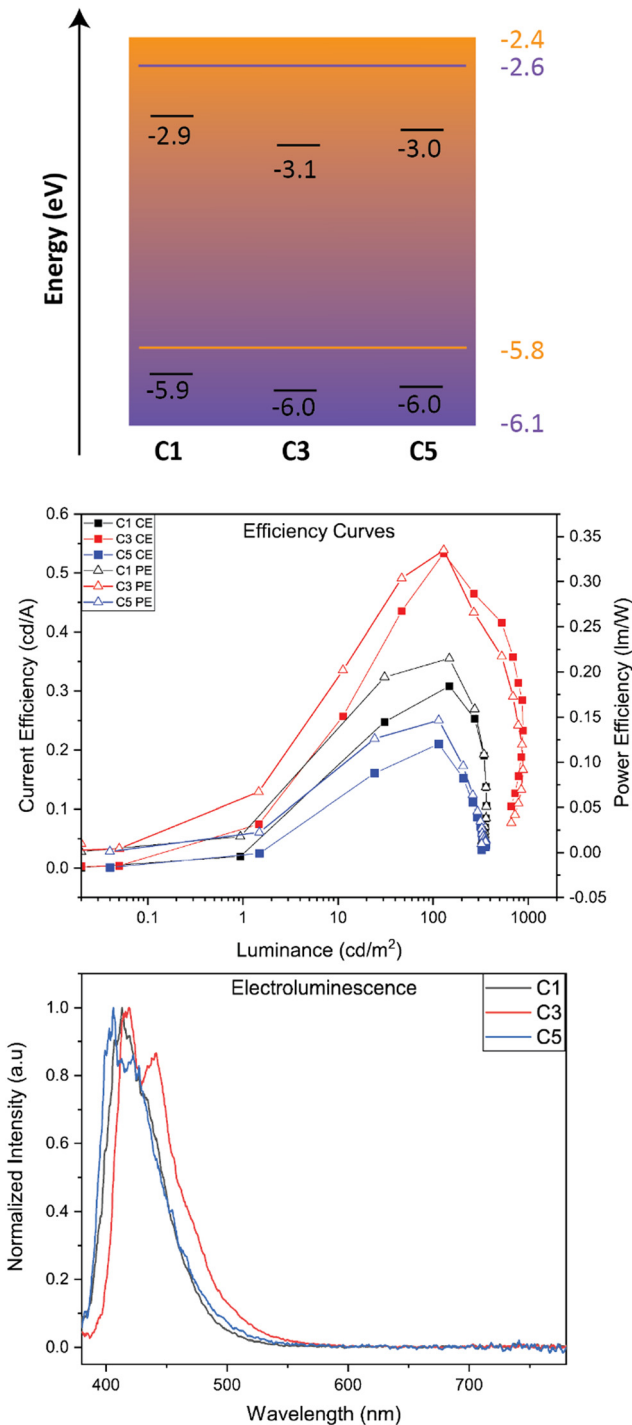
	$^{EL}\lambda_{max}$ (nm)	V_{100} (V)	L_{Max} (cd m^{-2})	CE_{Max} (cd A^{-1})	PE_{Max} (lm W^{-1})	EQE_{Max} (%)
	BBO					
Dopants	**C1**	**413**	4.3	363.4	0.308	0.215	0.874
	C3	**417, 441**	4.8	884.7	0.533	0.335	0.881
	C5	**405, 424**	4.4	358.6	0.210	0.147	0.538
Host	*m*CP	**481**	8.4	1247	0.106	0.033	0.049
	C2	**485**	4.4	1476	0.454	0.246	0.200
	C4	**484**	4.5	835.0	0.487	0.306	0.864
	C6	**486**	5.1	1200	0.915	0.448	0.356

$^{EL}\lambda_{max}$ = peak maxima of device. V_{100} = driving voltage at 100 cd m^{-2}. L_{Max} = maximum brightness. CE_{Max} = maximum current efficiency. PE_{Max} = maximum power efficiency. EQE_{Max} = maximum external quantum efficiency.

aryl substituents on a phenyl spacer conjugated to the BBO core effectively isolates the HOMO and LUMO. This pattern enhances the CT character of the materials and reduces the ΔE_{ST} of the molecule, but suppresses photoluminescence, reducing the PLQY of the system. Secondly, *para*-conjugation of the carbazole moieties result in the opposite effect where the LE character of the molecule is increased, reintroducing fluorescence but sacrificing TADF character. Fortuitously, **C1**, **C3**, and **C5** demonstrated attractive opto-electronic qualities as near-UV emitting generation 1 dopants while **C2**, **C4**, and **C6** were repurposed as ambipolar hosts. The solution-processed dopants demonstrated excellent near-UV emission ($CIE_y < 0.06$; $CIE_x = 0.16$) and competitive efficiencies to currently reported near-UV organic emitters. The BBO hosts paired with a commercial TADF emitter demonstrated reduced turn-on voltages and increased efficiencies in comparison to the p-type host, *m*CP. While these preliminary results show great promise for the candidates in the field of organic electronics, future works include further optimization of both sets of BBO materials using an evaporator with more extensive capabilities to attempt hyperfluorescent architectures (**C1**, **C3**, **C5**) and using the **C2**, **C4**, and **C6** as sensitizers for triplet recycling materials. Additionally, the TC group scaffold can be further improved to reintroduce fluorescent behaviour towards the production of TADF-active BBO emitters.

Experimental

Computational methodology

We generated initial 3D structures from SMILES[25] codes using the molconvert tool from ChemAxon. We then used the GFN-xTB[26] based conformer search algorithm CREST[27] to find the lowest energy conformers of all molecules. DFT based analysis of the molecules was done using the procedure described in Gómez-Bombarelli *et al.*[28] The optimized geometry of the lowest energy conformers was obtained from CREST on a B3-LYP/6-31G* level of theory[27,29] in gas phase and performed TDDFT calculations on the same level of theory to obtain HOMO and LUMO levels, permanent dipole moments, S_1 and $T1$ excitation energies as well as S_0 to S_1 transition dipole moments and oscillator strengths. We computed the TADF rates according to eqn (1) given in Gómez-Bombarelli *et al.*,[28] which depends on

Fig. 5 (top) Band diagram of active layer materials using BBO-based dopants. In purple are the HOMO/LUMO levels for 26DCzPPY while in orange is TCTA. (center) Power and current efficiency curves. (bottom) Normalized EL spectra.

DFT calculations suggested only three of the six BBOs could potentially exhibit TADF character. To confirm predictions, each material was synthesized in three steps and evaluated using a variety of steady-state and transient absorption spectroscopic techniques to understand their opto-electronic properties. The results indicate twofold. First, *meta*-conjugation of electron rich

the S_1 excitation energy, the S_1–T_1 gap and the oscillator strength for the S_0 to S_1 transition. We used $n = 1$ to be consistent with the data reported in Gómez-Bombarelli et al.[28] Using a more realistic n would not change the trends. All DFT calculations were done using the QChem package version 5.1.[30]

Materials and characterization

4,8-Dibromo-2,6-diethylbenzobisoxazole,[11] 2,5-diaminohyroquinone bishydrochloride,[31] and 4,6-dinitroresorcinol[32] were synthesized according to literature procedures. THF was dried using an Innovative Technologies solvent purification system. All other chemical reagents were purchased from commercial sources and used without further purification unless otherwise noted. Nuclear magnetic resonance (NMR) experiments were carried out in $CDCl_3$ at 500 MHz (^1H) AND 125 MHZ (^{13}C). In all spectra, chemical shifts are given in δ relative to residual protonated solvent peak, $CHCl_3$ (7.26 ppm, ^1H; 77.16 ppm, ^{13}C). Coupling constants are reported in hertz (Hz). High-resolution mass spectra were recorded on a double-focusing magnetic sector mass spectrometer using ESI. All UV-Vis and fluorescence spectra were obtained using quartz cuvettes with a 10 mm path length in $CHCl_3$ or as spin-casted thin films on a quartz slide (filtered 5 mg mL^{-1} solution in $CHCl_3$ spun at 1500 rpm). UV-vis spectra were collected on a Shimadzu UV-1800 UV spectrophotometer. Photoluminescence spectra were obtained on a Varian Cary Eclipse spectrophotometer. Absolute solution fluorescence quantum yields were obtained using a HORIBA spectrophotometer Nanolog FL3-2iHR equipped with a Quanta-phi integrating sphere. Ultraviolet photoelectron spectroscopy (UPS) was used to acquire the ionization potentials and approximate the HOMO values for each material. All substrates (positively doped silicon; 10 × 10 mm^2) had 40 nm of silver deposited via thermal evaporation. Samples were prepared by dissolution in $CHCl_3$ at a concentration of 5 mg mL^{-1} and stirred for a minimum of 4 h. Each solution was filtered to remove potential aggregates and sequentially spin-coated under a nitrogen atmosphere. Spectra were then acquired under ultrahigh vacuum at random positions on the formed film. The fluorescence quantum yields (ϕ) of the investigated compounds were calculated using the Williams comparative method.[1] A series of increasingly dilute solutions, with optical density starting at 0.10, were utilized for the calculations. The quantum yields were calculated using eqn (1):[33]

$$\phi = \phi_{STD} (Grad_x \, \eta_x^2)/(Grad_{STD} \, \eta_{STD}^2) \qquad (1)$$

where ϕ is the calculated quantum yield, η is the refractive index of the solvent, and Grad is the slope obtained from plotting the integrated fluorescence area vs. the optical density. The subscripts STD and x refer to the standard and investigated compound, respectively. Anthracene in cyclohexane was used as the standard for these calculations.[2,34] The method for obtaining oxygen-free ϕ was to purge oxygen from the solutions via nitrogen bubbling for ten minutes. The decay lifetimes of transient states were investigated via the nanosecond transient absorption (nsTAS) technique.[18,19] 3,4 A LP980 (Edinburgh) transient system was coupled with a Spectra-Physics QuantaRay Nd:YAG nanosecond puled laser and a GWU Optical Parametric

Oscillator tunable from 206–2600 nm for the excitation beam. For our purposes, the excitation beam was set to each sample's respective absorption maximum. A pulsed broadband xenon lamp beam was used to probe the excited states. These measurements were conducted in both oxygen rich and oxygen free solutions. The rate of reverse intersystem crossing (k_{rISC}) were calculated using eqn (2)[4,19]

$$k_{rISC} = k_{ESA} \, \phi_{TADF} \qquad (2)$$

where k_{ESA} is the decay rate of the triplet state and ϕ_{TADF} is the difference between purged and unpurged ϕ.

Synthesis of precursors

General SNAr procedure. To a flask equipped with condenser and stir-bar was added an appropriate amount of 9H-carbazole (1 mmol eq. for mono-fluorinated substrates, 2 mmol eq. for di-fluorinated substrates). The solid was dissolved in DMF to make a 1 M solution followed by the addition of an equivalent mmol amount of potassium tert-butoxide. This solution was brought to 60 °C under normal atmospheric conditions before the dropwise addition of the fluorinated benzonitrile or bromobenzene derivative. The solution was brought to reflux allowed to stir for a maximum of 24 hours. After cooling to room temperature, the reaction mixture was added to distilled water and stirred for 30 minutes before filtering the newly formed solid. For compounds **1** and **2**, the solid was dissolved in DCM, washed twice with distilled water, dried over Na_2SO_4, concentrated onto silica gel and purified by column chromatography (hex:DCM gradient). For compounds **3** and **4**, the solid was stirred in hot methanol, cooled to −20 °C and filtered to give the final product. Below are the following yields:

9-(4-Bromophenyl)-9H-carbazole (1). White solid. (86%). ^1H NMR (500 MHz, CDCl$_3$) δ 8.15 (d, J = 7.8 Hz, 2H), 7.74 (d, J = 8.6 Hz, 2H), 7.49–7.37 (m, 6H), 7.35–7.28 (dd, J = 8.0, 8.0 Hz, 2H).

9,9′-(5-Bromo-1,3-phenylene)bis(9H-carbazole) (2). White solid. (65%). ^1H NMR (500 MHz, CDCl$_3$) δ 8.16 (d, J = 7.8 Hz, 4H), 7.87 (d, J = 1.9 Hz, 2H), 7.80 (t, J = 1.9 Hz, 1H), 7.56 (d, J = 8.2 Hz, 4H), 7.51–7.44 (dd, J = 7.7, 1.2 Hz, 4H), 7.34 (t, J = 7.4 Hz, 4H).

4-(9H-Carbazol-9-yl)benzonitrile (3). White solid. (78%). ^1H NMR (500 MHz, CDCl$_3$) δ 8.17 (dt, J = 7.8, 1.0 Hz, 2H), 7.89–7.86 (m, 2H), 7.72–7.68 (m, 2H), 7.48–7.45 (m, 4H), 7.37 (ddd, J = 8.0, 5.1, 3.0 Hz, 2H).

3,5-Di(9H-carbazol-9-yl)benzonitrile (4). White solid. (71%). ^1H NMR (500 MHz, CDCl$_3$) δ 8.16 (d, J = 7.9 Hz, 4H), 8.07 (t, J = 2.0 Hz, 1H), 7.97 (d, J = 1.8 Hz, 2H), 7.56–7.48 (m, 8H), 7.38 (td, J = 7.4, 6.9, 1.4 Hz, 4H).

General procedure for boronic ester formation. To an oven-dried, N_2 filled flask was added approximately 40 mL of anhydrous THF and 8 mmol of corresponding bromobenzene derivative. This solution was cooled to −78 °C before the dropwise addition of 9.6 mmol of 2.5 M n-butyllithium. The organolithium species was allowed to stir at for 1 hour at before the dropwise addition of

12 mmol of 2-Isopropoxy-4,4,5,5-tetramethyl-1,3,2-dioxaborolane. The solution was allowed to come to room temperature for overnight stirring. Afterwards, 40 mL of distilled water and diethyl ether were added to the flask. The aqueous layer was separated, and the organic layer was then washed twice with distilled water, dried over Na_2SO_4, and concentrated onto silica gel. Column chromatography (hexanes: ethyl acetate gradient) was used to separate the product from impurities producing the following yields:

9-(4-(4,4,5,5-Tetramethyl-1,3,2-dioxaborolan-2-yl)phenyl)-9H-carbazole (5). Yellow viscous liquid (79%). ^{1}H NMR (500 MHz, CDCl$_3$) δ 8.16 (d, J = 7.7 Hz, 2H), 8.08 (d, J = 8.1 Hz, 2H), 7.62 (d, J = 8.2 Hz, 2H), 7.47 (d, J = 8.2 Hz, 2H), 7.42 (t, J = 7.6 Hz, 2H), 7.30 (t, J = 7.2 Hz, 2H), 1.42 (s, 12H).

9,9′-(5-(4,4,5,5-Tetramethyl-1,3,2-dioxaborolan-2-yl)-1,3-phenylene)-bis(9H-carbazole) (6). White solid. (60%). ^{1}H NMR (500 MHz, CDCl$_3$) δ 8.16 (d, J = 7.8 Hz, 4H), 8.13 (d, J = 2.1 Hz, 2H), 7.89 (t, J = 2.1 Hz, 1H), 7.52 (d, J = 8.2 Hz, 4H), 7.46 (ddd, J = 8.2, 7.1, 1.2 Hz, 4H), 7.32 (ddd, J = 7.5, 1.1 Hz, 4H), 1.38 (s, 12H).

General hydrolysis procedure. To a flask equipped with a stir-bar and condenser was added 10 mmol of benzonitrile. This solid was then suspended in 20 mL of 6 M NaOH and 20 mL of reagent grade ethanol and brought to reflux for overnight stirring. After cooling to room temperature, the reaction slurry was poured into cold 6 M HCl (excess) and stirred for 2 hours at room temperature. The solid was filtered and washed with 25 mL of cold water and 50 mL of cold methanol and allowed to dry under vacuum producing the following yields:

4-(9H-Carbazol-9-yl)benzoic acid (7). White solid. (95%). ^{1}H NMR (500 MHz, CDCl$_3$) δ 8.40 (d, J = 8.1 Hz, 2H), 8.16 (d, J = 7.8 Hz, 2H), 7.76 (d, J = 8.1 Hz, 2H), 7.53 (d, J = 8.2 Hz, 2H), 7.45 (t, J = 7.7 Hz, 2H), 7.34 (t, J = 7.4 Hz, 2H).

3,5-Di(9H-carbazol-9-yl)benzoic acid (8). White solid. (89%). ^{1}H NMR (500 MHz, CDCl$_3$) δ 8.46 (d, J = 2.0 Hz, 2H), 8.17 (d, J = 7.7 Hz, 4H), 8.11 (t, J = 2.0 Hz, 1H), 7.55 (d, J = 8.2 Hz, 4H), 7.47 (t, J = 7.7 Hz, 4H), 7.38 – 7.31 (t, J = 7.8 Hz, 4H).

General procedure for formation of C1 and C2. This precursor was prepared similar to literature procedures.[35] The general procedure is as follows: 0.2 mmol of 4,8-dibromo-2,6-diethylbenzobisoxazole was added to a 75 mL pressure flask along with 5% mol equivalent PEPPSI-iPr and 0.5 mmol of **5** or **6** and. To the same flask was added 1.3 mmol of cesium fluoride. These contents were dissolved in 10 mL of THF and degassed for 15 minutes. Afterwards, the flask was sealed and heated to 130 °C for 12 hours. After cooling to room temperature, the crude solution was diluted with DCM and concentrated onto silica gel for solid-loaded column chromatography using hexanes:CHCl$_3$ as the eluent to produce pure products.

4,8-Bis(4-(9H-carbazol-9-yl)phenyl)-2,6-diethylbenzo[1,2-d:4,5-d′]bis(oxazole) (C1). Pale-green solid (60%). M.P. > 240 °C. ^{1}H NMR (500 MHz, CDCl$_3$) δ 8.59 (d, J = 8.5 Hz, 4H), 8.19 (d, J = 7.7 Hz, 4H), 7.82 (d, J = 8.5 Hz, 4H), 7.62 (d, J = 8.2 Hz, 4H), 7.47 (ddd, J = 8.2, 7.1, 1.2 Hz, 4H), 7.33 (ddd, J = 7.9, 7.0, 1.0 Hz, 4H), 3.15 (q, J = 7.6 Hz, 4H), 1.58 (t, J = 7.6 Hz, 6H). ^{13}C NMR (126 MHz, CDCl$_3$) δ 169.18, 146.24, 140.77, 137.51, 137.17, 131.55, 131.52, 127.00, 126.00, 123.52, 120.33, 120.08, 113.32, 110.04, 77.26, 77.00, 76.75, 22.69, 11.37. HRMS (ESI) m/z: [M + H]$^+$ calcd for $C_{48}H_{35}N_4O_2$: 699.2760; found: 699.2778.

4,8-Bis(3,5-di(9H-carbazol-9-yl)phenyl)-2,6-diethylbenzo[1,2-d: 4,5-d′]bis(oxazole) (C2). Off-white solid. (37%). M.P. > 240 °C. ^{1}H NMR (500 MHz, CDCl$_3$) δ 8.64 (s, 4H), 8.19 (d, J = 7.7 Hz, 8H), 7.96 (s, 2H), 7.87 (d, J = 8.3 Hz, 8H), 7.49 (t, J = 7.7 Hz, 8H), 7.34 (t, J = 7.5 Hz, 8H), 3.11 (q, J = 7.7 Hz, 4H), 1.58 (t, J = 7.6 Hz, 6H). ^{13}C NMR unable to be obtained. HRMS (ESI) m/z: [M + H]$^+$ calcd for $C_{72}H_{49}N_6O_2$: 1029.3917; found: 1029.3954.

General procedure for the synthesis of C3–C6. To an oven-dried round bottom flask containing a stir-bar was added 1.00 g of P_2O_5. The flask was fitted with a condenser and purged with nitrogen three times followed by the addition of 4 mL of *o*-dichlorobenzene and 2.1 mL of hexamethyldisiloxane. These reagents were brought to reflux and stirred for 2 hours. To solution was cooled to appx. 80 °C. Next, 1.5 mmol of **7** or **8** and 0.5 mmol of DAHQ·2HCl were added quickly and simultaneous and the solution was heated to 190 °C for 2 days of stirring. Afterwards, the solution was cooled to room temperature and precipitated by pouring the mixture into methanol at −78 °C and filtered. The small molecules were purified according to methods A or methods B. Below, each molecules purification method is specified along with corresponding yields and characterization.

Method A – Compounds were passed through a hexanes: CHCl$_3$ plug. The solvent was removed, and crude material was then dissolved in CHCl$_3$ and decolorised with minimal activated charcoal. Filtering off the charcoal, the filtrate was then concentrated onto silica gel for purification *via* column chromatography (hex:CHCl$_3$ gradient).

Method B – Compounds were recrystallized twice in toluene using decolorizing carbon to remove black color. After filtering, the solid was spun in ample amounts of hot CHCl$_3$ and filtered three times.

2,6-Bis(4-(9H-carbazol-9-yl)phenyl)benzo[1,2-d:4,5-d′]bis(oxazole) (C3). Method A; pale green solid (28%). M.P. > 240 °C. ^{1}H NMR (500 MHz, CDCl$_3$) δ 8.54 (d, J = 8.5 Hz, 4H), 8.17 (d, J = 7.8 Hz, 4H), 8.02 (s, 2H), 7.81 (d, J = 8.5 Hz, 4H), 7.54 (d, J = 8.2 Hz, 4H), 7.46 (ddd, J = 8.2, 7.0, 1.3 Hz, 4H), 7.37–7.32 (ddd, J = 7.8, 6.8, 1.0 Hz, 4H). ^{13}C NMR (126 MHz, CDCl$_3$) δ 163.63, 148.78, 140.96, 140.67, 140.31, 129.27, 127.12, 126.21, 125.51, 123.82, 120.57, 120.47, 109.79, 101.14. HRMS (ESI) m/z: [M + H]$^+$ calcd for $C_{44}H_{27}N_4O_2$: 643.2134; found: 643.2139.

2,6-Bis(3,5-di(9H-carbazol-9-yl)phenyl)benzo[1,2-d:4,5-d′]bis(oxazole) (C4). Method B; grey solid (29%). M.P. > 240 °C. ^{1}H NMR (500 MHz, CDCl$_3$) δ 8.63 (s, 4H), 8.18 (d, J = 8.0 Hz, 8H), 8.03 (s, 2H), 7.97 (s, 2H), 7.62 (d, J = 8.0 Hz, 8H), 7.48 (t, J = 7.7 Hz, 8H), 7.35 (t, J = 7.7 Hz, 8H). ^{13}C NMR Unable to be obtained due to limited solubility. HRMS (ESI) m/z: [M + H]$^+$ calcd for $C_{68}H_{41}N_6O_2$: 973.3291; found: 973.3318.

2,6-Bis(4-(9H-carbazol-9-yl)phenyl)benzo[1,2-d:5,4-d′]bis(oxazole) (C5). Method A; pale yellow solid (35%). M.P. > 240 °C. ^{1}H NMR (500 MHz, CDCl$_3$) δ 8.53 (d, J = 8.1 Hz, 4H), 8.20 (s, 1H), 8.17 (d, J = 7.8 Hz, 4H), 7.88 (s, 1H), 7.81 (d, J = 8.2 Hz, 4H), 7.54 (d, J = 8.2 Hz, 4H), 7.46 (t, J = 7.6 Hz, 4H), 7.34 (t, J = 7.4 Hz, 4H). ^{13}C NMR (126 MHz, CDCl$_3$) δ 163.14, 149.10, 140.90, 140.32, 140.11, 129.20, 127.13, 126.21, 125.51, 123.81, 120.56, 120.47, 110.11, 109.79, 93.47. HRMS (ESI) m/z: [M + H]$^+$ calcd for C$_{44}$H$_{27}$N$_4$O$_2$: 643.2134; found: 643.2135.

2,6-Bis(3,5-di(9H-carbazol-9-yl)phenyl)benzo[1,2-d:5,4-d′]bis(oxazole) (C6). Method B; grey solid (38%). M.P. > 240 °C. ^{1}H NMR (500 MHz, CDCl$_3$) δ 8.62 (s, 4H), 8.18 (d, J = 8.0 Hz, 9H), 8.02 (s, 2H), 7.82 (s, 1H), 7.62 (d, J = 8.0 Hz, 8H), 7.48 (t, J = 7.6 Hz, 8H), 7.35 (t, J = 7.6 Hz, 8H). ^{13}C NMR Unable to be obtained due to limited solubility. HRMS (ESI) m/z: [M + H]+ calcd for C$_{68}$H$_{41}$N$_6$O$_2$: 973.3291; found: 973.3293.

Author contributions

David Wheeler: conceptualization, methodology, investigation, writing – original draft, writing – review & editing, and visualization. Pascal Friederich: investigation and data curation. Lloyd Fisher: investigation, writing – original draft, writing – review & editing. Angelar Muthike: investigation, writing – review & editing. Alán Aspuru-Guzik: conceptualization, methodology, investigation, and funding acquisition. Theodore Goodson: investigation, writing – review & editing, visualization and funding acquisition. Malika Jeffries-EL: conceptualization, methodology, investigation, writing – original draft, writing – review & editing, visualization supervision, project administration and funding acquisition.

Conflicts of interest

There are no conflicts to declare.

Acknowledgements

Notes and references

1 Y.-F. Liu, J. Feng, Y.-G. Bi, D. Yin and H.-B. Sun, *Adv. Mater. Technol.*, 2019, **4**, 1800371.

2 A. Zhou, H. Wang, Y. Zhang and C. Hu, *Fiber Integr. Opt.*, 2022, 1–25, DOI: 10.1080/01468030.2022.2083532; J. Song, H. Lee, E. G. Jeong, K. C. Choi and S. Yoo, *Adv. Mater.*, 2020, **32**, 1907539; C. Murawski and M. C. Gather, *Adv. Opt. Mater.*, 2021, **9**, 2100269.

3 R. Pode, *Renewable Sustainable Energy Rev.*, 2020, **133**, 110043; H. Sasabe and J. Kido, *Chem. Mater.*, 2011, **23**, 621–630; G. M. Phelan, *Inf. Disp.*, 2018, **34**, 10–15.

4 G. Gryn'ova, K.-H. Lin and C. Corminboeuf, *J. Am. Chem. Soc.*, 2018, **140**, 16370–16386; H. Bronstein, C. B. Nielsen, B. C. Schroeder and I. McCulloch, *Nat. Rev. Chem.*, 2020, **4**, 66–77; R. M. Pankow and B. C. Thompson, *Polymer*, 2020, **207**, 122874.

5 J. Tagare and S. Vaidyanathan, *J. Mater. Chem. C*, 2018, **6**, 10138–10173; M. Zhu and C. Yang, *Chem. Soc. Rev.*, 2013, **42**, 4963–4976; Z. Xu, B. Z. Tang, Y. Wang and D. Ma, *J. Mater. Chem. C*, 2020, **8**, 2614–2642; A. Monkman, *ACS Appl. Mater. Interfaces*, 2022, **14**, 20463–20467.

6 M. A. Baldo, D. F. O'Brien, Y. You, A. Shoustikov, S. Sibley, M. E. Thompson and S. R. Forrest, *Nature*, 1998, **395**, 151.

7 X. Cai and S.-J. Su, *Adv. Funct. Mater.*, 2018, **28**, 1802558; Y.-Z. Shi, H. Wu, K. Wang, J. Yu, X.-M. Ou and X.-H. Zhang, *Chem. Sci.*, 2022, **13**, 3625–3651.

8 C. A. Parker and E. J. Bowen, *Proceedings of the Royal Society of London. Series A. Mathematical and Physical Sciences*, 1963, **276**, 125–135; H. Uoyama, K. Goushi, K. Shizu, H. Nomura and C. Adachi, *Nature*, 2012, **492**, 234–238.

9 Y. Im, M. Kim, Y. J. Cho, J.-A. Seo, K. S. Yook and J. Y. Lee, *Chem. Mater.*, 2017, **29**, 1946–1963; I. Zoh, M. Imai-Imada, J. Bae, H. Imada, Y. Tsuchiya, C. Adachi and Y. Kim, *J. Phys. Chem. Lett.*, 2021, **12**, 7512–7518.

10 B. C. Tlach, A. L. Tomlinson, A. Bhuwalka and M. Jeffries-El, *J. Org. Chem.*, 2011, **76**, 8670–8681.

11 B. C. Tlach, A. L. Tomlinson, A. G. Ryno, D. D. Knoble, D. L. Drochner, K. J. Krager and M. Jeffries-El, *J. Org. Chem.*, 2013, **78**, 6570–6581.

12 D. L. Wheeler, A. V. Diodati, A. L. Tomlinson and M. Jeffries-El, *ACS Omega*, 2020, **5**, 12374–12384.

13 A. A. Burney-Allen, J. Shaw, D. L. Wheeler, L. Diodati, V. Duzhko, A. L. Tomlinson and M. Jeffries-El, *Asian J. Org. Chem.*, 2021, **10**, 215–223.

14 R. Chavez III, M. Cai, B. Tlach, D. L. Wheeler, R. Kaudal, A. Tsyrenova, A. L. Tomlinson, R. Shinar, J. Shinar and M. Jeffries-El, *J. Mater. Chem. C*, 2016, **4**, 3765–3773.

15 D. Wheeler, S. Tannir, E. Smith, A. Tomlinson and M. Jeffries-El, *Mater. Adv.*, 2022, **3**, 3842–3852; X. Yin, T. Zhang, Q. Peng, T. Zhou, W. Zeng, Z. Zhu, G. Xie, F. Li, D. Ma and C. Yang, *J. Mater. Chem. C*, 2015, **3**, 7589–7596.

16 Y. Sagara, K. Shizu, H. Tanaka, H. Miyazaki, K. Goushi, H. Kaji and C. Adachi, *Chem. Lett.*, 2015, **44**, 360; J. Lim, T. A. Albright, B. R. Martin and O. Š. Miljanić, *J. Org. Chem.*, 2011, **76**, 10207–10219.

17 J. Luo, S. Gong, Y. Gu, T. Chen, Y. Li, C. Zhong, G. Xie and C. Yang, *J. Mater. Chem. C*, 2016, **4**, 2442–2446.

18 R. J. Vázquez, H. Kim, P. M. Zimmerman and T. Goodson, *J. Mater. Chem. C*, 2019, **7**, 4210–4221.

19 R. J. Vázquez, J. H. Yun, A. K. Muthike, M. Howell, H. Kim, I. K. Madu, T. Kim, P. Zimmerman, J. Y. Lee and T. G. Iii, *J. Am. Chem. Soc.*, 2020, **142**, 8074–8079.

20 R. J. Vázquez, H. Kim, B. M. Kobilka, B. J. Hale, M. Jeffries-El, P. Zimmerman and T. Goodson, *J. Phys. Chem. C*, 2017, **121**, 14382–14392.

21 B. Carlotti, Z. Cai, H. Kim, V. Sharapov, I. K. Madu, D. Zhao, W. Chen, P. M. Zimmerman, L. Yu and T. Goodson, *Chem. Mater.*, 2018, **30**, 4263–4276; Z. Cai, R. J. Vázquez, D. Zhao, L. Li, W.-Y. Lo, N. Zhang, Q. Wu, B. Keller, A. Eshun, N. Abeyasinghe, H. Banaszak-Holl, T. Goodson and L. Yu, *Chem. Mater.*, 2017, **29**, 6726–6732; B. Keller, Z. Cai, A. K. Muthike, P. K. Sahu, H. Kim, A. Eshun, P. M. Zimmerman, D. Zhang and T. Goodson, *J. Phys. Chem. C*, 2018, **122**, 27713–27733.

22 S. Hirata, Y. Sakai, K. Masui, H. Tanaka, S. Y. Lee, H. Nomura, N. Nakamura, M. Yasumatsu, H. Nakanotani, Q. Zhang, K. Shizu, H. Miyazaki and C. Adachi, *Nat. Mater.*, 2015, **14**, 330.

23 L. Fisher, R. J. Vázquez, M. Howell, A. K. Muthike, M. E. Orr, H. Jiang, B. Dodgen, D. R. Lee, J. Y. Lee, P. Zimmerman and T. Goodson, *Chem. Mater.*, 2022, **34**, 2161–2175.

24 J. Tagare, R. Boddula, S. S. Sudheendran, D. K. Dubey, J.-H. Jou, S. Patel and S. Vaidyanathan, *J. Mater. Chem. C*, 2020, **8**, 16834–16844.

25 D. Weininger, *J. Chem. Inf. Comput. Sci.*, 1988, **28**, 31–36.

26 S. Grimme, C. Bannwarth and P. Shushkov, *Journal of Chemical Theory and Computation*, 2017, **13**, 1989–2009; C. Bannwarth, S. Ehlert and S. Grimme, *J. Chem. Theory Comput.*, 2019, **15**, 1652–1671.

27 P. Pracht, F. Bohle and S. Grimme, *Phys. Chem. Chem. Phys.*, 2020, **22**, 7169–7192.

28 R. Gomez-Bombarelli, J. Aguilera-Iparraguirre, T. D. Hirzel, D. Duvenaud, D. Maclaurin, M. A. Blood-Forsythe, H. S. Chae, M. Einzinger, D. G. Ha, T. Wu, G. Markopoulos, S. Jeon, H. Kang, H. Miyazaki, M. Numata, S. Kim, W. Huang, S. I. Hong, M. Baldo, R. P. Adams and A. Aspuru-Guzik, *Nat. Mater.*, 2016, **15**, 1120.

29 A. D. Becke, *J. Chem. Phys.*, 1993, **98**, 1372–1377.

30 Y. Shao, Z. Gan, E. Epifanovsky, A. T. B. Gilbert, M. Wormit, J. Kussmann, A. W. Lange, A. Behn, J. Deng, X. Feng, D. Ghosh, M. Goldey, P. R. Horn, L. D. Jacobson, I. Kaliman, R. Z. Khaliullin, T. Kuś, A. Landau, J. Liu, E. I. Proynov, Y. M. Rhee, R. M. Richard, M. A. Rohrdanz, R. P. Steele, E. J. Sundstrom, H. L. Woodcock, P. M. Zimmerman, D. Zuev, B. Albrecht, E. Alguire, B. Austin, G. J. O. Beran, Y. A. Bernard, E. Berquist, K. Brandhorst, K. B. Bravaya, S. T. Brown, D. Casanova, C.-M. Chang, Y. Chen, S. H. Chien, K. D. Closser, D. L. Crittenden, M. Diedenhofen, R. A. DiStasio, H. Do, A. D. Dutoi, R. G. Edgar, S. Fatehi, L. Fusti-Molnar, A. Ghysels, A. Golubeva-Zadorozhnaya, J. Gomes, M. W. D. Hanson-Heine, P. H. P. Harbach, A. W. Hauser, E. G. Hohenstein, Z. C. Holden, T.-C. Jagau, H. Ji, B. Kaduk, K. Khistyaev, J. Kim, J. Kim, R. A. King, P. Klunzinger, D. Kosenkov, T. Kowalczyk, C. M. Krauter, K. U. Lao, A. D. Laurent, K. V. Lawler, S. V. Levchenko, C. Y. Lin, F. Liu, E. Livshits, R. C. Lochan, A. Luenser, P. Manohar, S. F. Manzer, S.-P. Mao, N. Mardirossian, A. V. Marenich, S. A. Maurer, N. J. Mayhall, E. Neuscamman, C. M. Oana, R. Olivares-Amaya, D. P. O'Neill, J. A. Parkhill, T. M. Perrine, R. Peverati, A. Prociuk, D. R. Rehn, E. Rosta, N. J. Russ, S. M. Sharada, S. Sharma, D. W. Small, A. Sodt, T. Stein, D. Stück, Y.-C. Su, A. J. W. Thom, T. Tsuchimochi, V. Vanovschi, L. Vogt, O. Vydrov, T. Wang, M. A. Watson, J. Wenzel, A. White, C. F. Williams, J. Yang, S. Yeganeh, S. R. Yost, Z.-Q. You, I. Y. Zhang, X. Zhang, Y. Zhao, B. R. Brooks, G. K. L. Chan, D. M. Chipman, C. J. Cramer, W. A. Goddard, M. S. Gordon, W. J. Hehre, A. Klamt, H. F. Schaefer, M. W. Schmidt, C. D. Sherrill, D. G. Truhlar, A. Warshel, X. Xu, A. Aspuru-Guzik, R. Baer, A. T. Bell, N. A. Besley, J.-D. Chai, A. Dreuw, B. D. Dunietz, T. R. Furlani, S. R. Gwaltney, C.-P. Hsu, Y. Jung, J. Kong, D. S. Lambrecht, W. Liang, C. Ochsenfeld, V. A. Rassolov, L. V. Slipchenko, J. E. Subotnik, T. Van Voorhis, J. M. Herbert, A. I. Krylov, P. M. W. Gill and M. Head-Gordon, *Mol. Phys.*, 2015, **113**, 184–215.

31 M. Inbasekaran and R. Strom, *OPPI Briefs*, 1994, **23**, 447–450.

32 R. J. Schmitt, D. S. Ross, J. R. Hardee and J. F. Wolfe, *J. Org. Chem.*, 1988, **53**, 5568–5569.

33 A. T. R. Williams, S. A. Winfield and J. N. Miller, *Analyst*, 1983, **108**, 1067–1071.

34 I. B. Berlman, in *Handbook of Fluorescence Spectra of Aromatic Molecules*, ed. I. B. Berlman, Academic Press, 2nd edn, 1971, pp. 67–95, DOI: **10.1016/B978-0-12-092656-5.50009-5**.

35 A. K. Sharma, K. Gowdahalli, J. Krzeminski and S. Amin, *J. Org. Chem.*, 2007, **72**, 8987–8989.